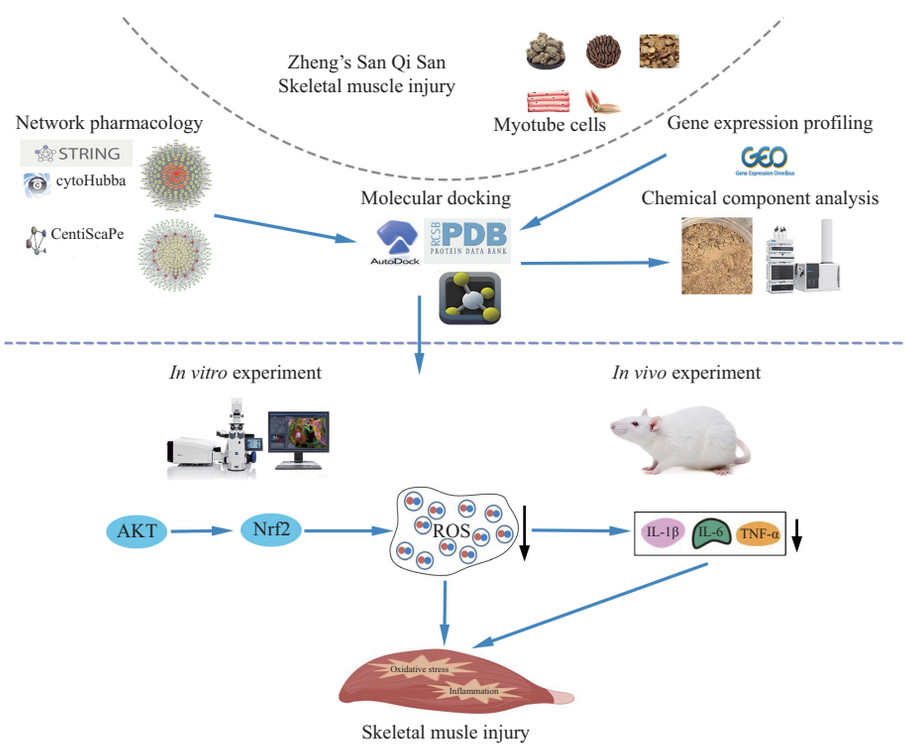
PIBB 生物化学与生物物理进展
Progress in Biochemistry and Biophysics
2026, 53(4): 1028~1047
www.pibb.ac.cn

Mechanistic Interpretation of Zheng's San Qi San Powder in Treating Skeletal Muscle Injury *via* Bioinformatics Prediction, Chemical Analysis and Experimental Verification*

WANG Ding-Rui[1)], LIU Yun-Xin[1)], XU Jun-Jie[2)], YANG Liu[1)], LÜ Jia-Hao[1)], XING Cheng-Yuan[1)], LÜ Lei[1)**], QIE Bei-Bei[1)**]

([1)]*Sports Medicine Key Laboratory of Sichuan Province, Institute of Sports Medicine and Health, School of Sports Medicine and Health, Chengdu Sport University, Chengdu* 641418, China;
[2)]*School of Clinical Medicine, Chengdu Medical College, Chengdu* 610500, China)

Graphical abstract



* This work was supported by grants from the General Program of Sichuan Science and Technology Education Joint Fund (2025NSFSC2102), Sichuan Provincial Undergraduate Training Program for Innovation and Entrepreneurship (S202510653119), and Research Excellence Program of Chengdu Sport University (2025-A007).
** Corresponding author.
LÜ Lei. Tel: 86-28-8509577, E-mail: lyulei@cdsu.edu.cn
QIE Bei-Bei. Tel: 86-28-85593740, E-mail: qiebeibei@cdsu.edu.cn
Received: September 25, 2025 Accepted: January 21, 2026

Abstract　**Objective**　Zheng's San Qi San (ZSQS) power, a classic traditional Chinese medicine (TCM) formula, is used for treating soft tissue injuries involving muscles, tendons, and ligaments. However, its underlying therapeutic mechanisms remain unclear. This study aimed to screen and identify pharmaceutically active ingredients and their candidate biomolecule targets, and further elucidate the molecular mechanism of ZSQS in the treatment of skeletal muscle injury. **Methods**　Network pharmacology was employed to construct "ZSQS-component-target", "protein-protein interaction (PPI)" and "active ingredient-core protein-pathway" networks to predict the key active ingredients and potential core targets of ZSQS for skeletal muscle injury. The predicted results were then validated *via* microarray data from the GEO database. Molecular docking was then performed to assess the binding ability between the screened active ingredients of ZSQS and the candidate core targets. Moreover, liquid chromatography-mass spectrometry (LC-MS) was used for qualitative and quantitative analysis to verify the active components of the drug and ZSQS serum. Finally, an animal model of eccentric exercise-induced skeletal muscle injury and a myotube cell model of oxidative stress-induced injury were established to validate the effects of ZSQS and its interventional effects on the biological functions of critical targets, thereby demonstrating the potential therapeutic mechanism of ZSQS. **Results**　Among the 111 active components identified in ZSQS and their corresponding 204 targets related to the skeletal muscle injury repair process, 14 core targets (including AKT1) and 4 core active components (quercetin, luteolin, kaempferol, and β-sitosterol) were screened out, while the corresponding metabolites of quercetin, luteolin and kaempferol were detected in the ZSQS serum. Among these targets, 5 candidate genes (*IL-6*, *CASP3*, *HIF1A*, *STAT3*, and *JUN*) overlapped with the differential expression screening results with GEO data, and IL-6 was confirmed to be enriched in the PI3K/AKT pathway. Combined with the prediction results of the AKT expression levels, these findings suggest that the phosphorylation level of AKT1 plays a core role in the therapeutic mechanism of ZSQS. Molecular docking analysis further revealed that the PH domain of AKT1 had high binding energy with all 4 core active components, as verified by LC-MS. Finally, animal model studies have shown the promoting effect of ZSQS administration on skeletal muscle injury repair and its possible antioxidant damage mechanism. Cell model studies further demonstrated that ZSQS-containing serum, core active ingredient combination therapy, and quercetin monomer could increase the phosphorylation level of AKT, promote the nuclear translocation of Nrf2, upregulate the expression of downstream antioxidant enzymes (SOD, GPx, and GR), and inhibit the expression of inflammatory factors (IL-6 and TNF-α), thereby alleviating oxidative stress and the inflammatory response. **Conclusion**　ZSQS alleviates skeletal muscle injury mainly by activating the AKT/Nrf2 signaling pathway, enhancing cellular antioxidant and anti-inflammatory capabilities. The results of this study provide a scientific basis for the clinical application and modernized development of ZSQS.

Key words　Zheng's San Qi San, skeletal muscle injury, AKT1, Nrf2, antioxidation, anti-inflammation
DOI：10.3724/j.pibb.2025.0421　　**CSTR**：32369.14.pibb.20250421

As a pivotal constituent of the human motor system, skeletal muscle orchestrates joint movement through precisely regulated contraction and relaxation processes[1]. Nevertheless, traumatic events (such as crush injuries or lacerations) or eccentric muscle contractions may damage skeletal muscle[2]. In such scenarios, local and recruited immune cells in the injured site detect damage-associated molecular patterns (DAMPs). Inflammatory cytokines released by recruited neutrophils stimulate myoblast fusion and vascularization to promote tissue repair. However, with the abundant release of inflammatory cytokines, significant production of reactive oxygen species (ROS) is initiated during inflammation[2-3]. The aberrant accumulation of ROS readily engages in reactions with proteins, lipids, carbohydrates, and nucleic acids, frequently resulting in irreversible functional impairments or even total cellular destruction[4]. Furthermore, ROS may activate inflammatory pathways such as the NF-κB pathway, thereby amplifying the expression of proinflammatory cytokines[5]. This establishes a detrimental cycle in which oxidative stress and inflammation mutually reinforce one another, leading to the aggravation of tissue injury[6]. Consequently, anti-inflammatory and antioxidant management has been demonstrated to be critical following skeletal muscle injury. Traditional physical therapy such as cryotherapy is believed to be able to modulate cellular metabolism and alleviate inflammation and oxidative stress in injured tissues; however, robust evidence-based support is lacking[7]. Nonsteroidal anti-inflammatory drugs (NSAIDs) are also commonly used for the treatment of muscle strain injuries. They effectively alleviate pain and inflammation, but increasing evidence suggests that NSAIDs may inhibit muscle regeneration, leading to long-term functional deficits such as weakened muscle fibers, fibrosis, and potential side effects due to increased leukotriene production[7]. Additionally, their clinical use is limited by adverse effects on the gastrointestinal tract, as well as potential renal and cardiovascular complications[8]. Antioxidants, despite their potential to counteract reactive oxygen species after muscle injury, exhibit conflicting effects in treating skeletal muscle damage. They may exacerbate injury by inhibiting cellular adaptation to exercise, but their roles in inflammation, strength loss, fatigue, and cell damage are unclear[9]. These limitations highlight

the need for safer and more effective therapeutic strategies.

Traditional Chinese medicine (TCM) has emerged as a critical modality in the clinical management of skeletal muscle injuries, because of its noninvasive, safe, and convenient characteristics[10]. Zheng's San Qi San (ZSQS), derived from "Selected Medical Writings of Zheng Huaixian", is a well-established formula used in treating soft tissue injuries involving muscles, tendons, and ligaments[11]. In this classical prescription, *Cyperus rotundus* L., the herb with the highest dosage, serves as the sovereign herb, complemented by *Panax notoginseng* and Licorice to activate blood circulation, dredge meridians, and nourish muscle tissues[12]. All the constituents of ZSQS exhibit anti-inflammatory and antioxidative properties. For example, *Cyperus rotundus* L. has been traditionally used in clinical practice to address various conditions, including diarrhea, diabetes, fever, inflammation, malaria, and gastrointestinal disorders[13]. Kilani-Jaziri *et al*[14]. confirmed that its extracts possess antioxidative capacity by inhibiting xanthine oxidase activity and lipid peroxidation in human leukemia cells. Similarly, *Panax notoginseng* exhibits extensive pharmacological activities, demonstrating efficacy in treating cardiovascular diseases, pain, inflammation, trauma, and both internal/external hemorrhage caused by injury[15], with its extracts showing antioxidative effects *in vitro*-cultured PC12 cells[16]. Liquorice, moreover, has been validated for its roles in respiratory regulation, immunomodulation, anti-neoplastic activity, anti-inflammation, gastrointestinal protection, and hepatoprotection[17]. The extracts also exhibit potent inhibitory effects on lipid oxidation in pork[18]. Therefore, understanding the pathophysiological process of skeletal muscle injury and the pharmacological mechanism of these potential therapies is crucial for promoting the repair of injured tissue, preventing secondary damage, and optimizing clinical strategies for safeguarding against skeletal muscle injury[19]. However, the complex composition of TCM formulas poses challenges, and the precise mechanisms underlying their multi-target synergistic actions remain poorly understood. This knowledge gap hinders standardization efforts and limits their broader international adoption and promotion.

Quercetin is a predominant flavonol naturally occurring in numerous plant species, including all the herbs in ZSQS[13,15,17]. It has been reported to possess anti-inflammatory and antioxidant properties *via* the PI3K/AKT, Nrf2, and MAPK pathways[20-24], which may contribute to the pharmacological features of ZSQS. In this study, along with the validation of involved signaling pathways and key therapeutic targets of ZSQS during skeletal muscle injury by bioinformatics methods, quercetin, luteolin, kaempferol, and β-sitosterol were identified as the core bioactive components by molecular interaction analysis with protein kinase B (AKT1) identified as a potential core target. Among these core components, quercetin exhibited the highest relative content. To explore the underlying mechanism, *in vitro* and *in vivo* skeletal muscle injury models were established. Utilizing these models, we have elucidated that ZSQS potentially exerts its therapeutic effects on skeletal muscle injury by enhancing antioxidant and anti-inflammatory capacities, an effect mediated through the AKT/Nrf2 signaling pathway.

1 Materials and methods

1.1 Bioinformatics analysis

1.1.1 Active ingredients and gene targets screening

ZSQS is composed of *Panax notoginseng* (40 g), Cyperi Rhizoma (processed with four adjuvants, 400 g), and Licorice (40 g). All herbal materials were pre-processed in accordance with standardized protocols for TCM herbal processing, then homogenized and pulverized into a fine powder. The recommended oral dosage for human adults is 2−4 g per administration, 2−3 times daily[12]. The TCMSP platform (https://test. tcmsp-e. com/) was used to retrieve the chemical components of ZSQS. The screening criteria included oral bioavailability (*OB*) ⩾ 30% and drug-likeness (*DL*) ⩾0.18. Finally, the corresponding target gene names were obtained from the Uniprot database (https://www.uniprot.org/) and restricted to human genes. Based on these data, the network of "ZSQS-component-target" was constructed using Cytoscape version 3.10.3.

1.1.2 Skeletal muscle injury-related targets screening

Effective target genes associated with skeletal muscle injury were collected from three databases, GeneCards (https://www.genecards.org/), OMIM (https://mirror.omim.org/), and DrugBank (https://go.drugbank.com/). The species was limited to *Homo sapiens*. Specifically, candidate targets retrieved from the GeneCards database were filtered using the median of the GeneCards Score, with genes exceeding this median identified as potential disease targets. Duplicate entries were removed to obtain the final set of complete skeletal muscle injury target genes. The skeletal muscle injury targets and the protein targets of ZSQS were input into the Venny online tool (https://bioinfogp.cnb.csic.es/tools/venny/) to generate a Venn diagram and identify the

intersection targets.

1.1.3 GO and KEGG enrichment analysis

The overlapping protein targets of ZSQS and skeletal muscle injury were uploaded to the DAVID database (https://david.ncifcrf.gov/) to conduct enrichment analyses, which included the biological processe (BP), molecular function (MF), and cellular component (CC) categories for Gene Ontology (GO) analysis. For Kyoto Encyclopedia of Genes and Genomes (KEGG) analysis, pathways were classified into five types, environmental information processing, human diseases, organismal systems, cellular processes and metabolism[25-26]. Enriched terms were ranked based on both the *P*-value<0.05 and gene count. Visualization was conducted using the Bioinformatics Tool (https://www.bioinformatics.com.cn/) to generate informative data visualizations.

1.1.4 The protein-protein interaction （PPI） network construction

The potential targets were imported into the STRING database (http://string-db.org/) to obtain PPI-related information, which was then retrieved from the database. Specifically, the analysis was conducted with *Homo sapiens* specified as the target organism and the minimum interaction score set to “medium confidence” (≥0.4). Then the resulting PPI network data was visualized using Cytoscape 3.10.3. Furthermore, core target screening was conducted using three topological algorithms within the CytoHubba plugin, maximum neighborhood component (MNC), maximal clique centrality (MCC), and edge percolated component (EPC) [26]. The intersection of the top 20 targets identified by each algorithm was used to determine the core hub genes.

1.1.5 Core ingredient screening

Cytoscape software was implemented to construct and visualize a comprehensive “component-target-pathway” network. In this network, components, targets, and pathways were visually distinguished by distinct node shapes and colors, while interactions between nodes were illustrated by connecting edges. Core components were identified as those with degree centrality (DC), betweenness centrality (BC), and closeness centrality (CC) values exceeding their respective averages[25], determined *via* Centiscape 2.2 Menu analysis in Cytoscape 3.10.3.

1.1.6 Synergism analysis of key components with PPI network perturbation

Target network characteristics of drugs denote the network properties among drug target proteins within the context of the human PPI network, with the average shortest pathlength (ASP) being one of the most commonly used metrics, which represents the minimum number of nodes between drug target proteins in the PPI network. Based on this shortest pathlength, the degree of perturbation exerted by drug targets on the PPI network can be reflected, thereby further assessing the therapeutic effect of a drug on diseases. Therefore, the ASP of key component (**1.1.5**) targets in the PPI network was utilized to calculate the perturbation degree of different combinations of key components, thus evaluating both the therapeutic characteristics of synergistic combinations of key components and their perturbation degree on the skeletal muscle injury-related PPI network.

The specific calculation method is as follows:

$$S(d_A, d_B) = \frac{1}{n_A \times n_B} \sum_{i=1}^{n_A} \sum_{j=1}^{n_B} \mathbf{distance}(i,j) \quad (1)$$

where d_A and d_B represents individual key ingredients. $S(d_A, d_B)$ denotes the ASP between the targets of component d_A and component d_B. n_A is the number of targets of component d_A, and n_B is the number of targets of component d_B. A larger value of $S(d_A, d_B)$ indicates a greater degree of perturbation exerted by the combinatorial components on the disease network, which implies a better therapeutic effect of this two-component combination[27].

1.1.7 Gene expression profiling

To derive the clinical implications of potential key targets, we queried the GEO database to investigate gene expression changes in skeletal muscle at 3 h following high-intensity eccentric exercise-induced skeletal muscle injury. The GEO dataset GSE23697 was employed to validate these key genes. Using the “Limma” R package, differentially expressed genes (DEGs) from GSE23697 were identified with screening criteria set as a fold change≥1.5 and an adjusted *P*-value<0.05[28]. Enrichment analyses were conducted using the DAVID database (https://david.ncifcrf.gov/). For data visualization, the bioinformatics tool was utilized to generate informative outputs, including clustered heatmaps, volcano plots, and visualizations for enrichment analyses.

1.1.8 Molecular docking

Core target protein structures were retrieved from the UniProt database. Those suitable for docking were selected based on criteria including domain coverage and structural resolution, and their corresponding structure files were downloaded from the RCSB PDB database (https://www.rcsb.org/). The 3D structures of active ingredients in SDF format were obtained from the PubChem database (https://pubchem.ncbi.nlm.nih.gov/). For protein preparation, non-target molecules were removed using PyMOL 2. The processed proteins were then converted to pdbqt

format using the prepare_receptor module of the ADFR Suite. Similarly, small molecules were converted to pdbqt format using the prepare_ligand module of the same suite. Molecular docking was performed using AutoDock Vina 1.2.7 with an exhaustiveness value of 25 and a grid spacing of 0.375 Å. The docking box was constructed by extending 1.5 Å beyond the known ligand binding site. If no binding site was predefined, whole-protein docking was carried out. The docking results were processed with OpenBabel 3.1.1 to extract optimal conformations, ensure consecutive atom numbering, standardize PDB formatting, optimize chain identifiers and ligand residue names, and finally generate complex PDB files. Protein-ligand interactions were analyzed using PLIP to produce pse files, and figures were prepared with PyMOL.

1.2 Preparation of ZSQS serum

All animal studies were conducted in compliance with the guidelines outlined in the NIH publication and the principles established by Chengdu Sport University for the use and care of laboratory animals. The animal experiments were approved by the Ethics Review Committee of Chengdu Sport University (Ethics Review No. 137, 2025). Twenty 6-week-old male specific pathogen-free (SPF)-grade Sprague-Dawley (SD) rats, weighing (200±10) g, were purchased from Chengdu Dashuo Biotechnology Co., Ltd. (License No. SCXK (Chuan) 2025-0030).

Following a 1-week acclimatization period, the rats were randomly assigned to two groups: a control group (n=10) and a ZSQS-treated group (n=10). The ZSQS-treated group received 1.26 g/kg of ZSQS dissolved in 0.5% CMC-Na *via* oral gavage every 12 h for 7 consecutive days, while the control group was administered an equal volume of 0.5% CMC-Na solution on the same schedule. 2 h post the final gavage administration, blood specimens were harvested from the abdominal aorta after the rats were anesthetized *via* intraperitoneal injection of 1% pentobarbital sodium at a dose of 50 mg/kg. Subsequently, all rats were humanely euthanized through exsanguination until the occurrence of cardiac and respiratory arrest. The blood samples were centrifuged at 3 000 r/min for 20 min at 4℃ to separate the serum, which was subsequently inactivated by incubation in a 56℃ water bath for 30 min and filtered through a 0.22-μm membrane for sterilization. The resulting serum was stored at −80℃ until further analysis.

1.3 Identification and quantification of active ingredients

20 mg of ZSQS powder was accurately weighed and mixed with 1 ml of a solvent working solution (methanol∶water, 7∶3). The mixture was sonicated at room temperature for 30 min, followed by centrifugation at 10 000 r/min for 5 min. For serum sample preparation, 500 μl of serum was combined with 1.5 ml of acetonitrile. The mixture was vortexed for 5 min and then centrifuged at 12 000 r/min for 5 min. The supernatant was collected and dried under a stream of nitrogen at room temperature. The resulting residue was reconstituted in 100 μl of acetonitrile and vortexed for 5 min.

The supernatant of ZSQS powder was filtered and collected for analysis using ultra performance liquid chromatography-orbitrap tandem mass spectrometry (UPLC-Orbitrap MS/MS, Q Exactive Focus, Thermo Fisher Scientific, MA, USA). Chromatographic separation was performed on a Waters ACQUITY UPLC® BEH C18 column (1.7 μm, 2.1 mm×100 mm). The column temperature was maintained at 40℃, and the flow rate was set at a constant 0.4 ml/min. The mobile phase employed a gradient elution system consisting of mobile phase A (ultrapure water containing 0.1% formic acid) and mobile phase B (acetonitrile containing 0.1% formic acid). Electrospray ionization (ESI) was employed as the ion source, with detection conducted in Full MS-ddMS² mode. Both positive and negative ion modes were scanned across a mass range of m/z 100−1 200. The MS1 resolution was set to 70 000, while the MS2 resolution was configured to 35 000. The ion source voltage was maintained at 3 kV, and a gradient collision energy protocol featuring 20 eV, 40 eV, and 60 eV was applied.

The major constituents of ZSQS, including quercetin, luteolin, kaempferol, and β-sitosterol, were quantified using high-performance liquid chromatography-triple quadrupole tandem mass spectrometry (HPLC-MS/MS, Triple Quad^{TM} 4500MD, AB SCIEX, MA, USA). Briefly, 1 mg of each standard compound was weighed and dissolved in a working solution (methanol∶water, 7∶3). After ultrasonic extraction for 5 min at room temperature, the reference standards were prepared *via* gradient dilution. Concurrently, 25 mg of ZSQS powder was processed using the identical procedure. Chromatographic separation was performed on an ACQUITY UPLC® BEH C18 column (1.7 μm, 2.1 mm×100 mm) with the column temperature maintained at 40℃ , and a constant flow rate of 0.3 ml/min was used with a mobile phase consisting of solvent A (ultrapure water containing 0.1% formic acid) and solvent B (acetonitrile containing 0.1% formic acid). For mass spectrometric analysis, ESI in

positive ion mode was employed. The parameters for the four target constituents are as follows, the parent ion masses (*m*/*z*) of luteolin, kaempferol, β-sitosterol, and quercetin were 287.055, 287.050, 397.38, and 303, respectively, with their corresponding product *m*/*z* being 153.010, 153.010, 397.38, and 153.010. A uniform dwell time of 100 ms was applied across all four analytes. Collision energies were set to 80.000 V for both luteolin and kaempferol, and 30.000 V for β-sitosterol and quercetin. Serum samples were analyzed by HPLC-MS/MS using a widely targeted metabolomics approach. The chromatographic and mass spectrometric conditions are detailed in Table S1.

1.4 *In vitro* analysis

1.4.1 Cell culture and treatment

C2C12 myoblasts (Wuhan Pricella Biotechnology Co., Ltd., Wuhan, China; Lot No. CL-0044) were maintained in Dulbecco's Modified Eagle's Medium (DMEM) supplemented with 10% (*v*/*v*) fetal bovine serum (FBS), 100 U/ml penicillin, and 100 mg/L streptomycin (Nanjing SenBeiJia Biological Technology Co., Ltd., Nanjing, China; Lot No. BC-CE-007). Cell cultures were incubated at 37℃ in a humidified atmosphere with 5% CO_2. For induction of myotube differentiation, when C2C12 cells reached 80%−90% confluency, the culture medium was replaced with differentiation medium consisting of DMEM containing 2% horse serum (Wuhan Pricella Biotechnology Co., Ltd., Wuhan, China; Lot No. 164215) and renewed every 24 h. After 4 d of differentiation, myotubes were grouped as follows, the blank normal group was treated with 20% normal serum derived from rats fed with CMC-Na, and all the rest groups were treated with 600 μmol/L H_2O_2. Following H_2O_2 treatment, the model group was supported with 20% normal serum; the positive control group with 20% normal serum, and 10 μmol/L monomethyl fumarate (MMF, Medchemexpress, NJ, USA, Lot No. HY-103252); the ZSQS group with varying concentrations of ZSQS serum, including 5% ZSQS serum plus 15% normal serum, 10% ZSQS serum plus 10% normal serum, and 20% ZSQS serum; the active ingredient combination group with 20% normal serum, 7 μmol/L quercetin (Sigma, MO, USA; Lot No. Q4951), 4.5 μmol/L kaempferol (Aladdin, Shanghai, China; Lot No. K107144), 4.5 μmol/L β-sitosterol (Aladdin, shanghai, China; Lot No. S111183), and 4 μmol/L luteolin (Aladdin, shanghai, China; Lot No. L107329), according to the relative contents of these ingredients in ZSQS powder; and the quercetin group with 20% normal serum, and 20 μmol/L quercetin. To explore the underlying signaling pathway, 10 μmol/L LY294002 (Topscience, Shanghai, China; Lot No. T2008) was co-administered with either quercetin or 20% ZSQS serum to inhibit the PI3K pathway. Myotubes were pre-treated with various drugs or ZSQS serum for 2 h prior to exposure to H_2O_2, which was maintained for 24 h.

1.4.2 Cell counting kit-8 assay

The cells were cultured in 96-well plates and pretreated with varying concentrations of ZSQS before being exposed to H_2O_2 for 24 h. After adding 10 μl of CCK-8 reagent (Biosharp, Hefei, China; Lot No. BS350B) to each well, the plates were incubated at 37℃ for 2 h. Absorbance was then measured at 450 nm using a microplate reader (ALLSHENG, Hangzhou, China).

1.4.3 Nuclear and cytoplasmic proteins preparation

Nuclear and cytoplasmic proteins were extracted using a commercial assay kit (Biosharp, Hefei, China; Lot No. BL670B). Briefly, cells were harvested by centrifugation at 800*g* for 3 min at 4℃. The cells were then washed twice with PBS and lysed in chilled mixed Buffer A (450 μl) and Buffer B (50 μl) for 30 min on ice. The cell lysates were centrifuged at 1 200*g* for 10 min. Subsequently, the top layer containing cytoplasmic protein extracts was transferred to a new tube. For nuclear protein extraction, the precipitate was first vortexed vigorously at maximum speed for 15 s, followed by incubation with 100 μl of chilled Buffer C on ice for 45 min with additional vigorous vortexing for 15 s at 10-min intervals. After centrifugation at 14 000*g* for 30 min at 4℃, the supernatant containing nuclear protein components was collected and transferred to a new tube.

1.4.4 Western blot

The protein concentrations of nuclear protein, cytoplasmic protein, and total protein from myotubes and tissues were quantified using a BCA assay kit (Biosharp, Hefei, China; Lot No. BL521C). Western blotting was performed to assess protein expression levels. Equal amounts of protein samples were first separated by 10% sodium dodecyl sulfate-polyacrylamide gel electrophoresis (SDS-PAGE) and then transferred onto polyvinylidene difluoride (PVDF) membranes (Millipore, Bedford, USA, Lot No. ISEQ00010). Membranes were blocked with 5% nonfat dry milk for 2 h at room temperature to prevent nonspecific binding. Primary antibody incubations were carried out overnight at 4℃ using the following antibodies: anti-AKT (1∶10 000, Affinity, Liyang, China, Lot No. AF6261), anti-phospho-AKT (Thr308) (1∶2 000, Affinity, Lot No. AF3262), anti-phospho-AKT (Ser473) (1∶2 000, Affinity, Lot No. AF0016),

anti-Nrf2 (1∶1 000, CST, MA, USA, Lot No. 12721S), anti-β-actin (1∶50 000, Abclonal, Lot No. AC026), and anti-lamin B1 (1∶5 000, Proteintech, Lot No. 12987-1-AP). After washing, membranes were incubated with HRP-conjugated goat anti-rabbit secondary antibody (1∶8 000, Abclonal, Lot No. AS014) for 2 h at room temperature. Protein bands were visualized using the ECL Plus chemiluminescence detection system (Millipore, Lot No. WBKLS0100).

1.4.5 RT-qPCR

Total RNA was isolated from myotubes and tissues using Trizol reagent following the manufacturer's instructions. The purified RNA was reverse-transcribed into cDNA with the PrimeScript RT Reagent Kit (Takara, Kyoto, Japan; Lot No. RR047A). Quantitative real-time PCR was performed using Universal SYBR qPCR Master Mix (Biosharp, Hefei, China; Lot No. BL697A) on an Applied Biosystems QuantStudio 6 system. Primer sequences used in this study are detailed in Table S2. Beta-actin (Actb) was used as the internal control. The relative mRNA expression levels of the target genes were quantified using the $2^{-\Delta\Delta Ct}$ method.

1.4.6 ROS assay

C2C12 myotubes were pre-treated with various drugs or ZSQS-containing serum for 2 h before being exposed to H_2O_2. Following this treatment, the cells were incubated with 10 μmol/L ROS working solution (Biyuntian Biotechnology, Shanghai, China; Lot No. S0034S) at 37℃ for 20 min. Finally, they were washed three times with PBS and observed under a fluorescence microscope (Olympus, Tokyo, Japan).

1.4.7 Oxidative stress detection

C2C12 myotubes were homogenized, and total proteins were collected. The levels of superoxide dismutase (SOD) (Biyuntian Biotechnology, Shanghai, China; Lot No. S0101S), glutathione reductase (GR) (Biyuntian Biotechnology, Shanghai, China; Lot No. S0055), glutathione peroxidase (GPx) (Biyuntian Biotechnology, Shanghai, China; Lot No. S0057S), and glutathione (GSH) (Biyuntian Biotechnology, Shanghai, China; Lot No. S0053) in C2C12 myotubes were determined following the instructions provided with the biochemical assay kits from Biyuntian Biotechnology.

1.4.8 Immunofluorescence

Immunofluorescence staining was performed on C2C12 myotubes to evaluate the nuclear translocation of Nrf2. Cells were seeded onto coverslips in 24-well plates and cultured to allow differentiation. After treatment, cells were fixed with 4% paraformaldehyde (room temperature (RT), 10 min), permeabilized with 0.1% Triton X100 (RT, 15 min) and blocked with 5% BSA in PBS (RT, 30 min) before incubation with a primary antibody against Nrf2 (1∶400, CST, MA, USA, Lot No. 12721S) overnight at 4℃. Following three 5-min washes with PBS, coverslips were incubated with an Alexa Fluor 488-conjugated goat anti-rabbit secondary antibody (1∶500, Proteintech, Wuhan, China, Lot No. RGAR002) for 1 h at room temperature in the dark. Nuclei were counterstained with DAPI using an anti-fade mounting medium (Beyotime, Shanghai, China, Lot No. P0131). Fluorescent images were acquired using a confocal laser scanning microscope (Nikon, AXR NSPARC, Japan) with identical exposure settings across all samples.

1.5 *In vivo* experiments

1.5.1 Intervention process

Thirty SD rats, purchased from Dashuo (as detailed in **1.2**), were randomly assigned to 5 groups: placebo-treated sedentary group (CON), placebo-treated downhill running group (Down-Plac), dimethyl fumarate (DMF) -treated downhill running group (Down-DMF), ZSQS low-dose (ZSQS-L)-treated downhill running group (Down-ZSQS-L), and ZSQS high-dose (ZSQS-H) -treated downhill running group (Down-ZSQS-H).

Rats in the Down-ZSQS-L (0.63 g/kg, twice daily) and Down-ZSQS-H (1.26 g/kg, twice daily) groups received ZSQS (dissolved in 0.5% CMC-Na) *via* gavage. The experimental doses of ZSQS were determined based on the recommended dose for a 60-kg adult (4 g, 3 times daily) in clinical practice[12]. Rats in the CON and Down-Plac groups were administered an equal volume of 0.5% CMC-Na. Rats in the Down-DMF group received DMF at a dose of 150 mg/kg twice daily[29-30]. All drugs or the placebo were administered for 5 consecutive days prior to downhill running. After exercise, each group of animals was maintained on the same treatment for an additional 2 d[31].

The exercise protocol consisted of 90 min of intermittent downhill running on a motorized treadmill. After a brief familiarization with the protocol, the rats completed 18 intervals of 5-min running at 16 m/min along a 16° downward incline, with 2-min rest periods between each interval[31-32]. When required, a soft-bristled brush was used to stimulate their tails to encourage running. Animals that cannot meet the exercise requirement will be excluded from the group.

1.5.2 Analysis of blood and muscle biochemical indicators

48 h post-exercise, rats were anesthetized and blood collected from the jugular vein. Serum was

obtained after clotting at room temperature for 30 min, followed by centrifugation at 3 000 r/min for 15 min at 4℃. Serum creatine kinase (CK; Abbkine Sci. Co., Ltd., Wuhan, China; Lot No. KTB1012) and lactate dehydrogenase (LDH; Lot No. KTB1110) levels were determined with commercial assay kits. For soleus muscle samples, tissue was rinsed with PBS and homogenized with a homogenizer per the manufacturer's protocol. Following centrifugation of the homogenate, the supernatants were collected for the determination of SOD, GPx, GR, GSH, and malondialdehyde (MDA; Abbkine Sci. Co., Ltd., Wuhan, China; Lot No. KTB1050).

1.5.3 Transmission electron microscope （TEM） analysis

For TEM analysis, soleus muscle samples were fixed in 3% glutaraldehyde (4℃, 24 h) and postfixed with 1% osmium tetroxide (4℃, 2 h). A progressive dehydration series was implemented using acetone gradients (30%, 50%, 70%, 80%, 90%, 95%, followed by three 100% acetone rinses), with each concentration step lasting 10 min at RT. The specimens were subsequently infiltrated with acetone-Epon 812 resin mixtures at progressive ratios (3∶1, 1∶1, and 1∶3) before final embedding in pure Epon 812 resin. Ultrathin sections (60−90 nm) were sectioned using an ultramicrotome, floated on distilled water, and transferred to copper grids. Following dual staining with uranyl acetate (15 min) and lead citrate (2 min) at room temperature, the grids were imaged using a JEM-1400FLASH transmission electron microscope (JEOL, Japan).

1.6 Statistical analysis

Statistical analyses were performed using GraphPad Prism 10. Intergroup differences were assessed with Student's *t*-test for comparisons between two groups. For multi-group analyses, one-way analysis of variance (ANOVA) was applied. Continuous variables are expressed as mean±standard deviation (SD), and statistical significance was defined as a two-tailed $P<0.05$.

2 Results

2.1 Active ingredients in ZSQS and potential targets for the treatment of skeletal muscle injury

Following an exhaustive search of the TCMSP database, 118 active ingredients corresponding to 3 Chinese herbs in the ZSQS prescription were initially identified, with ingredients lacking human target information excluded from the dataset. Ultimately, 111 active ingredients were selected for subsequent research, among which A1, A2, B1-B4, C1, and D1 were found to be shared across multiple herbs while the remaining components were unique to individual ones (Table S3).

Gene target screening suggested that liquorice was associated with 1 385 potential targets, *Panax notoginseng* with 236, and *Cyperus rotundus* L. with 467. After removing duplicates, a final subset of 244 gene targets was obtained (Figure 1a, Table S4).

In parallel, 5 729 potential gene targets related to skeletal muscle injury were retrieved from the GeneCards, OMIM, and DrugBank databases (Table S5), and the 204 overlapping targets between ZSQS and skeletal muscle injury were subsequently displayed with a Venn diagram (Figure 1b, Table S6).

2.2 GO and KEGG pathway enrichment analysis of the drug−disease intersection targets

In order to perform biological functions and pathways on the 204 drug-disease intersection targets, the David database was used for the GO and KEGG analysis. GO analysis revealed that these targets were associated with 670 BP terms, 100 CC terms, and 181 MF terms. The top 10 significantly enriched GO terms were then selected from the BP, CC, and MF categories, respectively. These targets were primarily involved in biological processes such as "signal transduction", "response to xenobiotic", "inflammatory response", cellular components like "plasma membrane" and "cytosol", and molecular functions including "protein binding" and "protein kinase binding" (Figure S1e). KEGG pathway analysis identified 181 enriched pathways, which were categorized into 5 distinct groups: 24 pathways related to environmental information processing (Figure S1a), 83 pathways associated with human diseases (Figure S1b), 1 pathway linked to metabolism (Figure S1c), 14 pathways pertaining to cellular processes (Figure S1c), and 59 pathways involved in organismal systems (Figure S1d). Among these, the PI3K/AKT, MAPK, NF-κB, and TNF signaling pathways are involved in inflammation and oxidation processes, which supported the pharmacological mechanism related to ZSQS that is worth further investigation.

2.3 Core target screening and synergistic combination analysis

To further screen the core drug targets, a PPI network was constructed. The 204 overlapping targets were uploaded to the STRING database and visualized by Cytoscape 3.10.2. The resulting analysis contained 204 nodes and 4 660 edges, representing interactions with a confidence score exceeding 0.4 (Figure S2a). Subsequently, the cytoHubba plugin was utilized, employing its EPC (Figure S2b), MNC

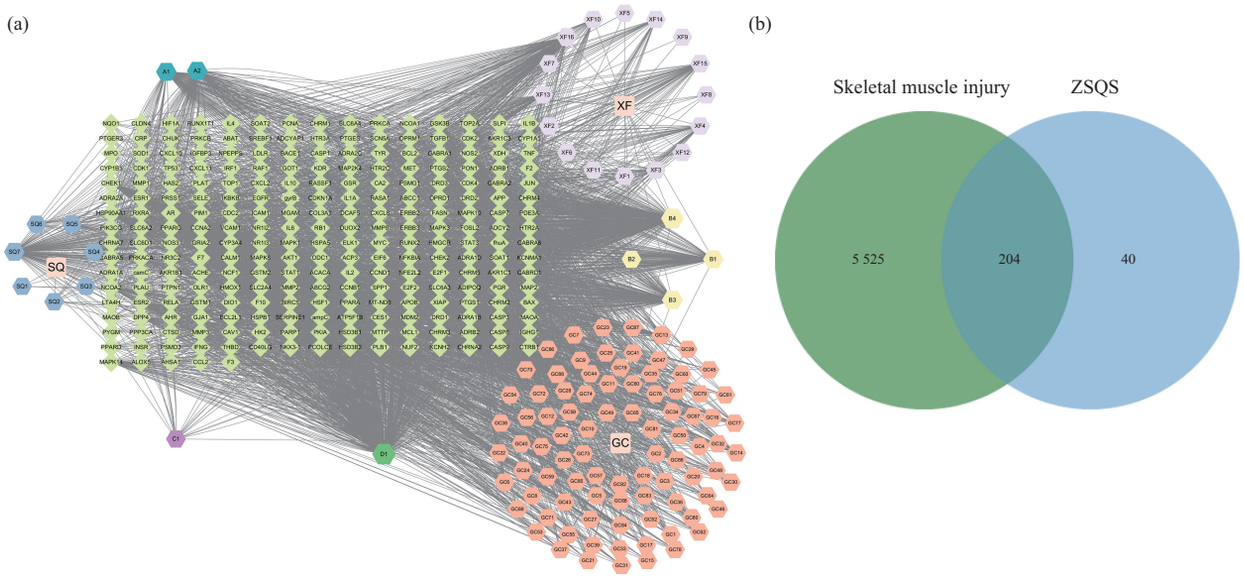


Fig. 1　Screening of potential targets of ZSQS in the treatment of skeletal muscle injury

(a) Component-target network of ZSQS. A total of 111 ZSQS active ingredients (circular nodes) were identified from the TCMSP database and 244 targets they modulated were isolated (diamond nodes). (b) Venn diagram showing the common targets affected by the active ingredients of ZSQS and the skeletal muscle injury process. SQ: Sanqi; XF: Xiangfu; GC: Gancao; A: shared Sanqi/Xiangfu; B: shared Xiangfu/Gancao; C: shared Sanqi/Gancao; D: shared ingredients of all herbs.

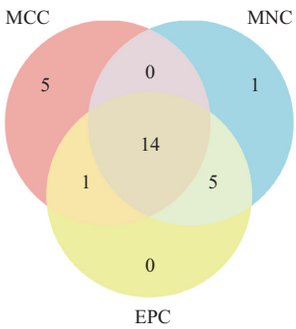
(Figure S2c), and MCC (Figure S2d) algorithms to identify the top 20 targets. Cross-analysis of these results revealed 14 targets, which were designated as hub targets (Figure 2a). These key targets included AKT1, matrix metallopeptidase 9 (MMP9), Caspase 3 (CASP3), transforming growth factor-β1 (TGF-β1), interleukin-1β (IL-1β), epidermal growth factor receptor (EGFR), prostaglandin-endoperoxide synthase 2 (PTGS2), interleukin-6 (IL-6), hypoxia inducible factor 1 subunit alpha (HIF1A), BCL2 apoptosis regulator (BCL2), tumor necrosis factor (TNF), proto-oncogene c-Jun (JUN), signal transducer and activator of transcription 3 (STAT3), and tumor protein P53 (TP53).

Furthermore, a ZSQS-active ingredient-hub target-pathway network was constructed by Cytoscape with the above-mentioned 14 core targets and KEGG enriched pathways containing these targets, including inflammatory and oxidative stress-related signaling cascades such as PI3K/AKT, MAPK, NF- κB, and TNF signaling pathways (Figure 2b). By setting a threshold higher than the average value of DC, BC and CC, the top 4 active ingredients within this network, including luteolin, quercetin, kaempferol, and β-sitosterol, were identified (Figure 2b). A further synergistic combination analysis was performed to predict the synergistic effects of these active ingredients. 6 distinct combinations were identified, with their corresponding synergistic scores are presented in Figure 2c. Among these, the quercetin-β-sitosterol and kaempferol-β-sitosterol combinations both exhibited the highest score. Collectively, these 4 constituents were confirmed as the key bioactive components of ZSQS in the treatment of skeletal muscle injury and were thus selected for further analysis.

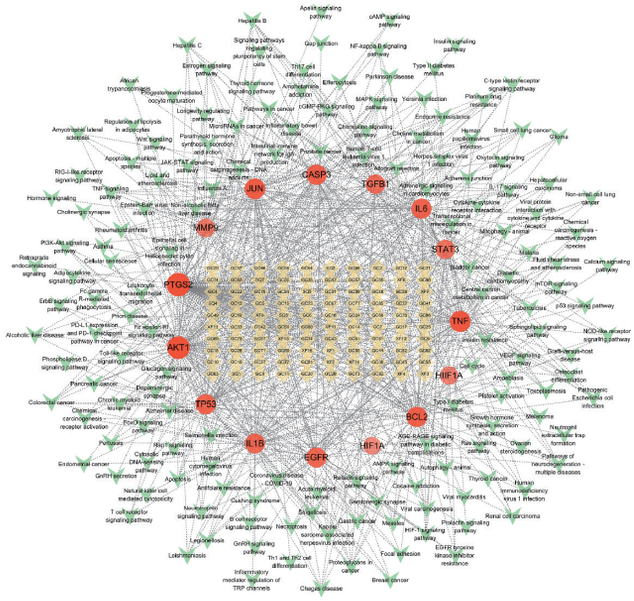
2.4　DEG identification of drug−disease intersection targets *via* microarray data analysis

In order to obtain biological evidence supporting the above screening results, microarray data analysis was first employed. A total of 70 high-quality microarray datasets were retrieved from the GEO database, encompassing 35 specimens from control legs and 35 from exercised legs in a paired-sample experiment. All participating subjects performed 100 eccentric contractions of the knee extensor muscles which can induce skeletal muscle injury[33]. To enhance the visualization of the DEG profile, a volcano plot was constructed using the criteria of fold change≥1.5 and P<0.05 (Figure S3a). Heatmaps were generated to display the DEGs, which consisted of 1 073 upregulated genes and 258 downregulated genes (Figure S3b). Among these DEGs, 5 genes, including *CASP3*, *HIF1A*, *STAT3*, *IL-6*, and *JUN*,

(a)



(b)



(c)

Ingredient-1	Ingredient-2	S(A,B)
Quercetin	β-Sitosterol	2.14
Kaempferol	β-Sitosterol	2.14
Luteolin	β-Sitosterol	1.96
Quercetin	Kaempferol	1.92
Luteolin	Kaempferol	1.84
Quercetin	Luteolin	1.83

Fig. 2　Screening of core targets and active ingredients

(a) Venn diagram view of overlapping hub targets screened using MNC, MCC, and EPC methods. (b) The ZSQS-active component-hub target-pathway network. (c) Synergism analysis result of the 4 key ingredients. MNC: maximum neighborhood component; MCC: maximal clique centrality; EPC: edge percolated component.

overlapped with the core targets predicted by network pharmacology. Notably, IL-6, a well-characterized myokine whose levels are elevated in diverse instances of exercise-induced muscle damage[34], was found to be enriched in the PI3K-AKT signaling pathway through KEGG enrichment analysis (Figure S3c, Table S7). Based on these evidences, we predicted that AKT1, a core target identified in the network pharmacology analysis, may exert anti-inflammatory functions by regulating IL-6 expression after muscle injury *via* post-translational regulation (such as phosphorylation). Collectively, these findings suggest that the functional role of AKT in skeletal muscle injury may be mediated by post-translational regulation rather than the alternation of its expression level, providing a foundation for subsequent functional investigations.

2.5　Molecular docking validation of AKT1 and the candidate active ingredients

To validate the reliability of AKT1 as a target for ZSQS in the treatment of skeletal muscle injury, molecular docking simulations were conducted between the four active ingredients and AKT1. All tested ingredients demonstrated strong binding activity with AKT1. β-Sitosterol exhibited the highest affinity (−9.71 kcal/mol), primarily through extensive hydrophobic interactions with TRP-80, THR-82, LYS-268 and VAL-270. The docking score of luteolin with AKT1 was −9.24 kcal/mol. It formed hydrogen bonds with GLN-79 and THR-211, a π-π stacking interaction with TRP-80, and hydrophobic interactions with TYR-272 and TRP-80. Both quercetin and kaempferol shared an identical binding energy of −9.08 kcal/mol. Specifically, quercetin binds to AKT1 *via* hydrogen bonds with ASN-54, THR-211 and VAL-271, a π-π stacking interaction with TRP-80. In contrast, kaempferol interacts with AKT1 *via* a π-π stacking interaction with TRP-80, along with hydrogen bonds to ASP-292, LEU-210, and SER-205, and hydrophobic interactions involving TRP-80, SER-205, LEU-264, VAL-270, and ASP-292 (Figure 3). Among these binding regions, ASN-54, GLN-79, TRP-80 and THR-82 are located within the PH domain. This domain is a critical structural component that governs the “PH-in” and “PH-out” conformational states of AKT, and is essential for the subsequent phosphorylation-dependent activation of the kinase[35].

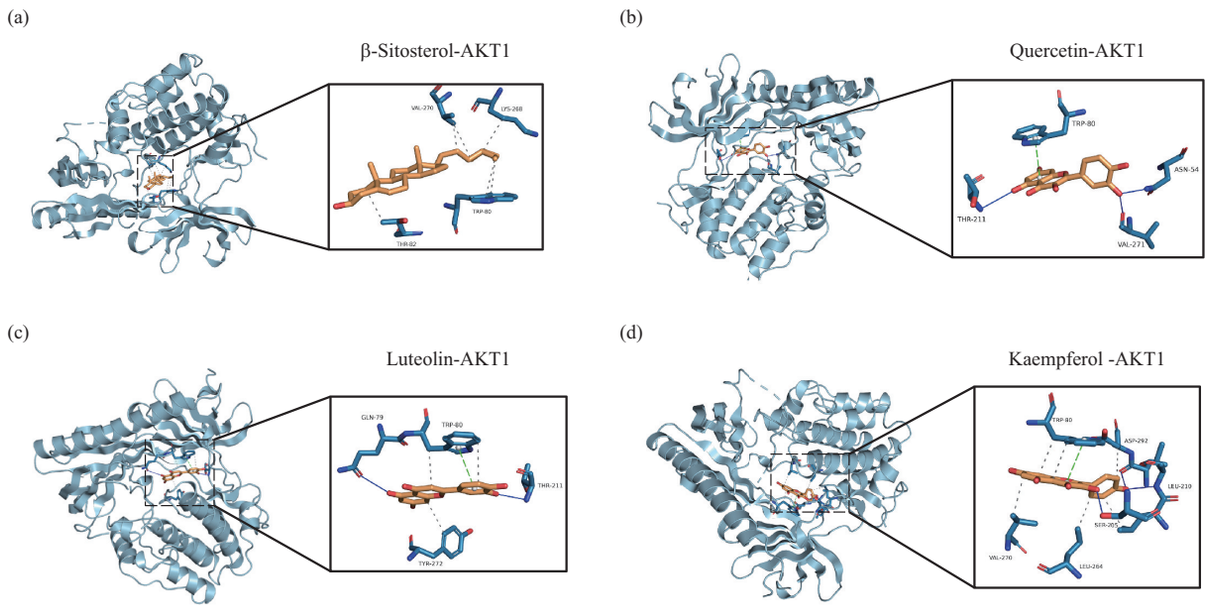


Fig. 3 Molecular docking between the core ingredient (ligand) of ZSQS and AKT1 (receptors)

The 3D spatial environment between β-sitosterol, quercetin, luteolin, or kaempferol and AKT1. The blue solid line represents hydrogen bonds, the gray dashed line represents hydrophobic interactions, and the green dashed line represents π-π bonds.

2.6 Verification of the core compounds of the ZSQS powder *via* LC−MS

To verify the presence of core compounds predicted in network pharmacology analyses, the chemical composition of ZSQS powder was characterized using LC-MS. Mass spectrometric analysis revealed that a total of 196 chemical constituents in the drug powder were matched with entries in the TCMSP database (Table S8). Among these, 4 key compounds, quercetin, luteolin, kaempferol, and β-sitosterol, were specifically identified (Figure 4). Quantitative analysis revealed that quercetin exhibited the highest relative content, at approximately 0.75 mg/g. Both kaempferol and β-sitosterol were detected at around 0.5 mg/g, followed by luteolin with a content of 0.47 mg/g (Figure S4). Subsequent analysis in ZSQS-containing serum identified 10 drug-related chemical constituents, including three glucuronide metabolites derived from quercetin, kaempferol, and luteolin, respectively (Table S9, Figure S5), indicating the possible pharmacological effects of these core components of ZSQS with their corresponding soluble metabolites.

2.7 ZSQS alleviates H_2O_2−induced oxidative stress *in vitro*

To verify the above drug-disease intersection prediction, an *in vitro* oxidative stress injury model was first established by employing H_2O_2 in C2C12 myotubes, aiming to mimic skeletal muscle damage induced by excessive physical exercise[36-38]. Our preliminary experiments showed that treatment with 600 μmol/L H_2O_2 resulted in excessive ROS production in myotubes after 24 h (data not shown). Subsequently, we established an oxidative stress cell model by stimulating C2C12 myotubes with 600 μmol/L H_2O_2. The CCK-8 assay first revealed that the cell viability of the model group was significantly lower than that of the normal control group (P<0.001) (Figure 5a). In comparation, cell viability showed an upward trend with the addition of ZSQS serum, and became significantly higher than that in the model group when serum concentration reached up to 20% (P<0.05), suggesting that serum from rats with oral administration of ZSQS could alleviate H_2O_2-induced injury.

We then evaluated the antioxidant effect of ZSQS-containing serum and the combination of 4 active ingredients in H_2O_2-induced C2C12 myotubes. In addition, the effect of quercetin was also detected based on its high synergistic interaction score and its content in the powder (Figure 2c, Figure 4). The DCFH-DA fluorescent probe was employed to detect ROS generation in these myotube groups. We did not observe a more pronounced antioxidant effect in the combination group (Figure S6); therefore, the ZSQS-containing serum and the selected monomer groups were employed for subsequent analysis. Fluorescence

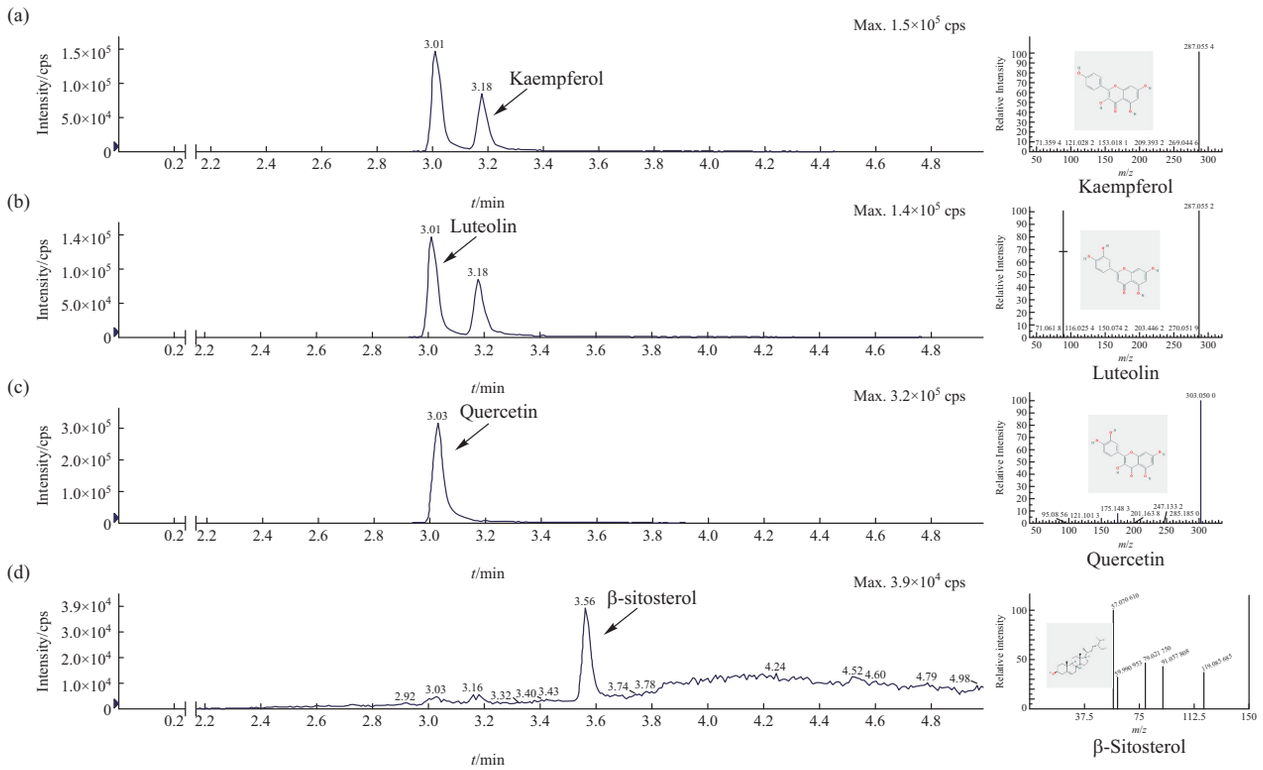


Fig. 4　Four core ingredients identified *via* mass spectrometry in the ZSQS powder sample

Kaempferol (a), luteolin (b), quercetin (c), and β-sitosterol (d) were identified in the ZSQS powder sample *via* positive-ion mode mass spectrometry, as shown on the left. The corresponding mass-charge ratio (*m*/*z*) values are presented on the right.

assays revealed that intervention with quercetin (P<0.001) or ZSQS-containing serum (P<0.001) significantly reduced ROS production, though to a lesser extent than the positive control group treated with MMF (P<0.001) (Figure 5b), a metabolite of DMF that has been reported to activate the Nrf2 pathway, which in turn enhances cytoprotection and mitigates skeletal muscle mass loss induced by oxidative stress[39-40]. Additionally, MMF, quercetin and ZSQS serum treatments significantly reversed the H_2O_2-induced decreases in the activities of SOD, GSH-px, GR as well as the levels of GSH (Figure 5c−f). In conclusion, these findings indicate that ZSQS may exert a protective effect against H_2O_2-induced oxidative stress in C2C12 myotubes, likely by inhibiting oxidative stress pathways.

2.8　ZSQS protects against H_2O_2−induced oxidative stress through the AKT/Nrf2 signaling pathway

On the basis of the observed protective effect against oxidative stress, the antioxidant mechanism of ZSQS was further investigated. According to the aforementioned bioinformatics analysis, AKT1 was predicted to be a potential core target of ZSQS in the treatment of skeletal muscle injury. This key target was involved in regulating the expression of downstream antioxidant enzymes by facilitating the nuclear translocation of Nrf2[41]. Thus, the expression and phosphorylation levels of AKT in these treatment groups were first analyzed. Western blotting analyses revealed a consistent trend in total AKT expression across all experimental groups (Figure 6a, b). By comparison, H_2O_2 treatment caused a significant decrease in AKT phosphorylation levels at both Thr308 (P<0.001) and Ser473 (P<0.001) sites. Notably, intervention with ZSQS serum or quercetin remarkably rescued the decreased phosphorylation levels caused by the presence of H_2O_2, albeit to a lesser extent than the MMF group (P<0.001 for all interventions). In contrast, LY294002, a PI3K inhibitor known to suppress AKT activation[42-43], reversed the elevated AKT phosphorylation levels in both ZSQS serum and quercetin treatment groups (Figure 6a, b), consistent with the observation that the same inhibitor abrogated the reduction of ROS production as well as the increased GSH levels and SOD, GPx, and GR activities in ZSQS serum and quercetin treated C2C12 myotubes (Figure 5b−f).

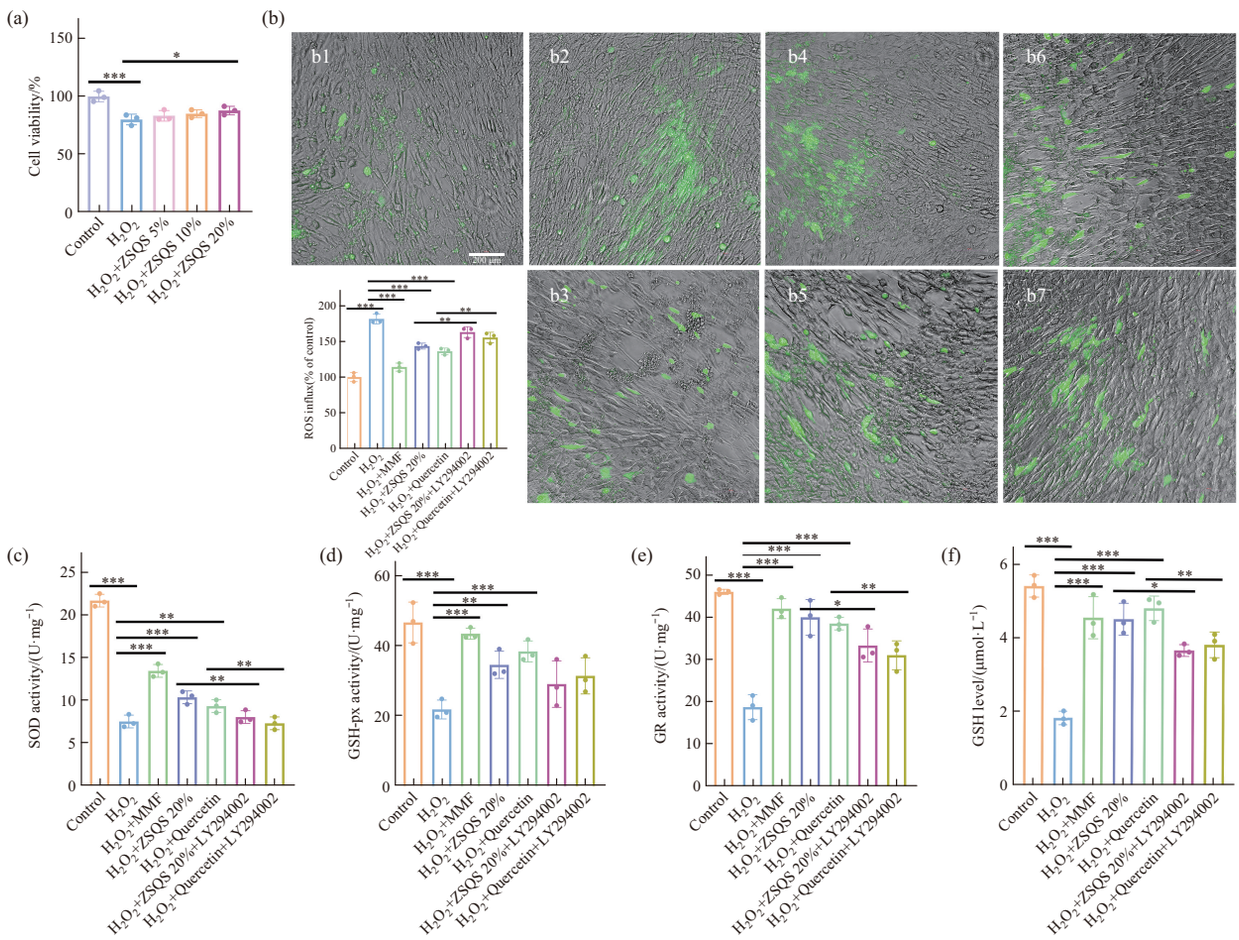


Fig. 5　Pharmacodynamic effects of ZSQS on H_2O_2−induced oxidative damage in C2C12 myotubes

(a) Cell viability of C2C12 myotubes detected by a CCK-8 assay. The cells were left untreated (control), or treated with 600 μmol/L H_2O_2 alone (H_2O_2), or in combination with ZSQS serum at concentrations of 5%, 10%, or 20%. (b) ROS levels in different groups of C2C12 myotubes were visualized *via* fluorescence microscopy (b1−b7), and quantified by measuring the mean fluorescence intensity. (b1) Control group; (b2) H_2O_2 group; (b3) H_2O_2+MMF group; (b4) H_2O_2+ZSQS 20%; (b5) H_2O_2+Quercetin; (b6) H_2O_2+ZSQS 20%+LY294002; (b7) H_2O_2+Quercetin+LY294002. (c−f) The levels of SOD, GSH, GSH-px, and GR in different groups of C2C12 myotubes were measured by the corresponding kits. The data are presented as mean±SD. **P*<0.05, ***P*<0.01, ****P*<0.001.

Aligned with the increased phosphorylation of AKT, elevated nuclear Nrf2 levels were also observed in ZSQS serum and quercetin treatment groups as well as the MMF positive control group (Figure 6a, b). Immunofluorescence staining further supported the strong Nrf2 nuclear translocation induced by ZSQS serum and quercetin (Figure 6c). And again, these translocations were reversed upon the suppression of AKT (Figure 6c).

Collectively, these findings demonstrate that ZSQS and its active ingredients trigger AKT signal transduction, which in turn promotes Nrf2 activation in order to promote the expression of downstream antioxidative proteins, thereby mitigating H_2O_2-induced oxidative stress[41,44].

2.9　ZSQS attenuates the H_2O_2−induced inflammatory response

During skeletal muscle injury, oxidative stress and inflammation act as mutually reinforcing processes[6]. Therefore, we further evaluated the interventional effect of ZSQS on H_2O_2-induced inflammatory responses. As illustrated in Figure S7, compared with the control group, treatment with 600 μmol/L H_2O_2 in cell model led to increased expression of inflammatory factors, including IL-6, IL-1β, TGF-β1, and TNF-α. Consistent with the above findings, both quercetin and ZSQS reversed the upregulation of IL-6 and TNF-α, suggesting that ZSQS and its active ingredients attenuate H_2O_2-induced inflammatory responses, which may be

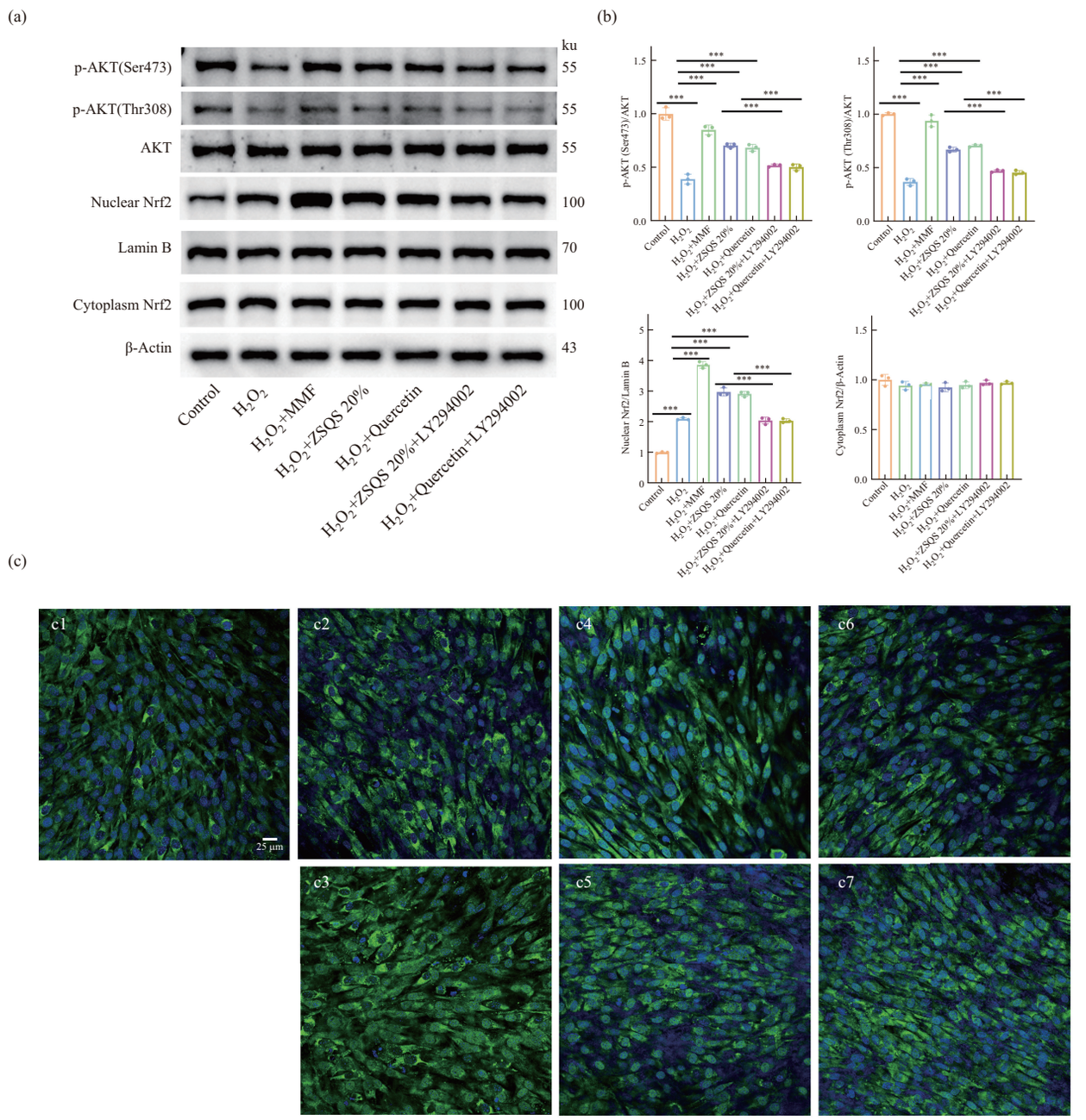


Fig. 6　ZSQS modulates the antioxidant effect *via* AKT/Nrf2−related pathways

(a) Representative Western blot image showing the protein expression levels of AKT, nuclear Nrf2, and cytoplasmic Nrf2, as well as the phosphorylation levels of AKT at Thr308 (AKT T308) and Ser473 (AKT S473) in C2C12 myotubes across treatment groups. (b) Quantitative analysis of the protein expression and phosphorylation levels shown in (a). (c) Immunofluorescence images showing the changes in the localization of Nrf2 (green) in C2C12 myotubes, with corresponding nuclear staining using DAPI (blue). (c1) Control group; (c2) H_2O_2 group; (c3) H_2O_2+MMF group; (c4) H_2O_2+ZSQS 20% ; (c5) H_2O_2+Quercetin; (c6) H_2O_2+ZSQS 20%+LY294002; (c7) H_2O_2+Quercetin+LY294002. The data are presented as mean±SD. ***P<0.001.

associated with AKT/Nrf2-regulated antioxidant capacity.

2.10　ZSQS alleviates eccentric exercise−induced muscle tissue damage and oxidative stress

To further validate the findings obtained from the aforementioned studies *in vivo*, a rat model of skeletal muscle injury was established using a 90 min intermittent downhill running (eccentric contraction) method[31-32]. Compared with the CON group, the exercise group (Down-Plac) exhibited significantly

elevated serum level markers of skeletal muscle damage, including CK (P<0.01) and LDH (P<0.001). In contrast, both low-dose and high-dose ZSQS treatments significantly reduced CK and LDH levels in these exercise groups (both P<0.05), though less pronounced than that observed in the DMF-treated positive control group (Figure 7a). These findings were consistent with the ultrastructural observation that the damage of myofibers induced by eccentric exercise was partly restored by both ZSQS and DMF treatment (Figure 7b).

Next, the oxidative stress levels were assessed in the soleus muscle tissue, a region that sustains greater muscle damage following downhill running[31-32]. ZSQS administration exhibited a dose-dependent capacity to reverse the exercise-induced reduction in antioxidant levels and the elevation of MDA, a major by-product and toxic mediator of oxidative stress, following exercise treatment (Figure 7c). In conclusion, our findings indicate that ZSQS exerts a protective effect against eccentric exercise-induced skeletal muscle tissue damage, probably through the suppression of oxidative stress.

2.11 ZSQS alleviates eccentric exercise−induced skeletal muscle injury *via* the AKT/Nrf2 signaling pathway

Soleus muscle tissues were further examined to confirm the role of AKT/Nrf2 signaling pathway during the antioxidant process of ZSQS. Consistent with the observations in cell model, while total AKT expression remained largely unchanged in the muscle, the phosphorylation levels of AKT at Thr308 (P< 0.001) and Ser473 (P<0.01) residues were significantly reduced in the exercise group, and these reductions were markedly reversed in both low-dose and high-dose ZSQS treatment groups (Figure 7d). Furthermore, compared with the exercise group, nuclear Nrf2 expression was significantly elevated in the ZSQS-L (P<0.05) and ZSQS-H (P<0.01) tissues, while cytoplasmic Nrf2 levels were decreased in the ZSQS-H group (P<0.05). Moreover, the elevated level of the pro-inflammatory cytokine IL-6 (P<0.05) in the Down-Plac group was significantly attenuated by both ZSQS-L (P<0.01) and ZSQS-H (P<0.001), whereas the elevated IL-1β level in the Down-Plac group (P< 0.05) was alleviated specifically in the ZSQS-H group (P<0.01) (Figure 7e).

Collectively, these findings demonstrate that ZSQS administration activates the AKT/Nrf2 signaling pathway, thereby suppressing eccentric exercise-induced skeletal muscle injury through the alleviation of oxidative stress and inflammatory responses.

3 Discussion

Muscle fiber damage caused by physical force or strenuous exercise, particularly lengthening contractions, elicits a rapid sequence of innate immune responses aimed at clearing damaged tissues, a process termed sterile inflammation, which is characterized by a pathophysiological state that significantly disrupts the cellular balance between oxidative stress and antioxidant defense[3, 5]. Inflammatory cytokines upregulate adhesion molecules (VCAM-1, CINC-1, and MCP-1) and NOS early in injury and activate ROS-generating enzymes (COX-2, NADPH oxidase, XO) through receptor binding. Moreover, injured muscle endothelial cells secrete TNF-α, IL-1, IL-6, and IL-8, forming a positive feedback loop[45]. During the respiratory burst phase, ROS generated by neutrophil NADPH oxidase deplete GSH. Conversely, sufficient GSH levels exert a partial inhibitory effect on the inflammatory process[46-47]. Consistent with this phenomenon, our *in vitro* experiments revealed that H_2O_2-treated C2C12 myotubes exhibited increased ROS, decreased GSH, and reduced activity of related antioxidant enzymes (SOD, GPx, and GR) (Figure 5). In contrast, ZSQS exhibited significant therapeutic effect towards these processes, manifested as reduced levels of oxidative markers and elevated the activity of antioxidant enzymes in the model treated with ZSQS-containing serum (Figure 5). Furthermore, the levels of inflammatory markers, including IL-6 and TNF-α, were decreased following ZSQS-containing serum treatment (Figure S7).

Owing to the inherent complexity of TCM, the molecular mechanisms underlying the therapeutic effects of ZSQS remain poorly understood. Network pharmacology has emerged as a robust methodology for identifying bioactive components and elucidating the mechanisms of TCM formulations. When integrated with molecular docking simulations, microarray data analysis and LC/MS-based chemical profiling, this combinatorial approach enables efficient and cost-effective exploration of the comprehensive component-target interactions that underpin the efficacy of ZSQS in treating skeletal muscle injury[48].

In this study, we screened 111 active ingredients of ZSQS from the TCMSP database. Subsequently, 204 overlapping targets between these ingredients in ZSQS and the skeletal muscle injury process were selected for further analysis. Based on these screening results, PPI network analysis identified AKT1, BCL2,

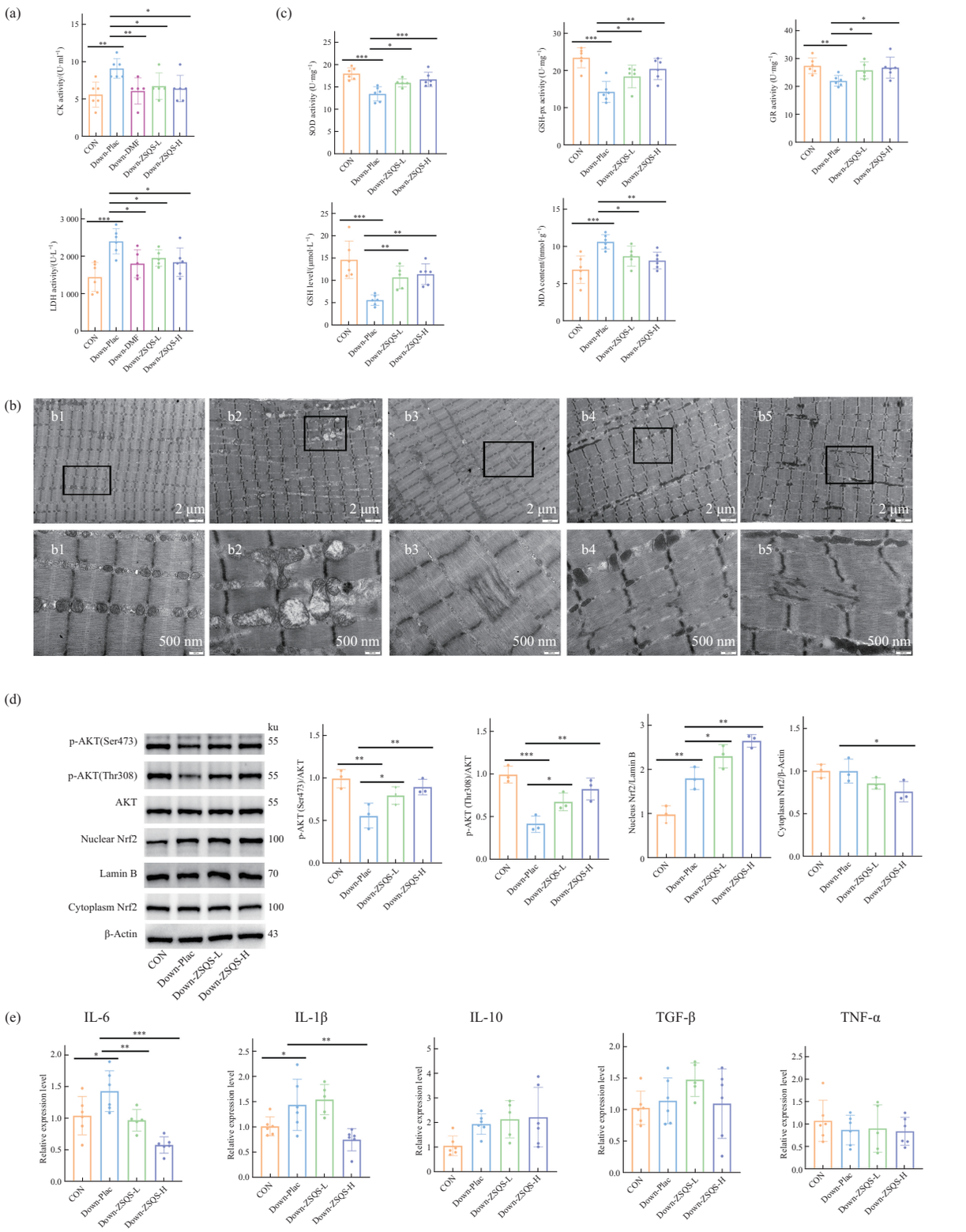


Fig. 7　ZSQS attenuates eccentric exercise−induced skeletal muscle damage and ameliorates oxidative stress and inflammatory responses *via* the AKT/Nrf2 signaling pathway

(a) Serum levels of CK and LDH in each group of rats. (b) Representative transmission electron microscopy images of soleus muscle myofibrils at the end of the intervention (upper panel: 8 000× magnification; lower panel: 30 000× magnification of the black-boxed region). (b1) CON; (b2) Down-Plac; (b3) Down-DMF; (b4) Down-ZSQS-L; (b5) Down-ZSQS-H. (c) Levels of SOD, GSH-px, GR, GSH and MDA in soleus muscle tissue measured with corresponding assay kits. (d) Representative Western blot showing protein expression of AKT, nuclear Nrf2, and cytoplasmic Nrf2, as well as phosphorylation of AKT at Thr308 (p-AKT T308) and Ser473 (p-AKT S473) in soleus muscle across groups. (e) RT-qPCR analysis of inflammatory-factor mRNA levels in soleus muscle. Data are presented as mean±SD; **P*<0.05, ***P*<0.01, ****P*<0.001.

CASP3, EGFR, HIF1A, IL-1β, IL-6, JUN, MMP9, PTGS2, STAT3, TGF-β1, TNF, and TP53 as the core targets of ZSQS in counteracting skeletal muscle injury, while ZSQS-active component-hub target-pathway network suggested that quercetin, luteolin, β-sitosterol, and kaempferol were identified as the primary active ingredients. Consistent with our GO and KEGG analysis, accumulating evidence indicates that the PI3K/AKT pathway plays a critical role in ameliorating oxidative stress and inflammation through the regulation of the transcription factor Nrf2[41,47,49]. The phosphorylation of PI3K and AKT facilitates the nuclear translocation of Nrf2, which further activates the expression of downstream antioxidant enzymes such as SOD, GPx, and GR. Additionally, activation of the Nrf2 pathway may exert anti-inflammatory effects by reducing excessive ROS production[47]. These findings suggest that the anti-inflammation and antioxidation therapeutic effect of ZSQS during skeletal muscle injury may be achieved primarily through modulation of the PI3K-AKT signaling pathway. This hypothesis underscores the need for further research to elucidate the specific role of this pathway in the alleviation of skeletal muscle injury by ZSQS.

Additionally, analysis of microarray data from the GEO database identified the differentially expressed gene IL-6, a factor related to muscle injury, is enriched in the PI3K-AKT signaling pathway (Figure S3). We speculate that AKT1 may be a key target involved in the pharmacological effects of ZSQS, potentially through post-translational regulatory mechanism. According to the molecular docking results (Figure 3), all four ingredients could bind to AKT1 and engage with its PH domain. In the inactive state of the kinase, the inhibitory “PH-in” conformation is relieved upon engagement of the PH domain with PI3K products, triggering a transition to the active “PH-out” conformation[35,50]. Given this mechanism and the observed binding specificity, these identified active ingredients from ZSQS may mimic the function of PI3K products to activate AKT1.

Consistent with the aforementioned screening and prediction results, analyses revealed a significant increase in AKT phosphorylation at both Thr308 and Ser473 in response to 20% ZSQS serum treatment in both cellular and animal models (Figure 6, 7). Concomitantly, we observed enhanced nuclear localization of Nrf2 (Figures 6, 7), which in turn activated the downstream expression of antioxidant enzymes (Figure 5). Collectively, these results suggest that elucidating the detailed mechanisms by which inflammatory factors and ROS contribute to skeletal muscle damage and repair may provide a molecular basis for the clinical application of ZSQS, not only in attenuating muscle injury and promoting repair, but also in preventing secondary damage[19]. Notably, in the cellular model, the antioxidative efficacy of the combined therapy with multiple active ingredients was comparable to that of ZSQS serum and the quercetin monotherapy (Figure S6). Given that the dosage of each individual ingredient in the combined therapy group was relatively lower than that in the quercetin group, this finding thereby indicates a potential synergistic effect of the combined treatment. However, the absence of superior therapeutic efficacy in the combined therapy group relative to the quercetin monotherapy *in vitro* may be attributed to two factors: first, the combined therapy may rely on complex *in vivo* metabolic processes involving these active ingredients and other auxiliary components in ZSQS; second, the high quercetin concentrations employed in *in vitro* experiments could mask the synergistic effects of the combined treatment[25]. Furthermore, KEGG analysis revealed the involvement of other anti-inflammatory and antioxidative pathways, including the MAPK signaling pathway, and NF-κB signaling pathway. These findings provided a supplement to the mechanistic results in this study by which ZSQS regulates skeletal muscle injury and implied that the complete therapeutic effects may attribute to the multi-ingredient and multi-target mechanism, which aligns with the unique advantage of TCM’s holistic therapeutic philosophy that needs further investigation (Figure S8).

Our study has limitations that warrant consideration. First, the hypothesized molecular interaction between the core components and the key target AKT1 requires validation through point mutation experiments. Second, future studies employing conditional knockout models or pathway-specific pharmacological modulators will be crucial to confirming the therapeutic potential and biological significance of this regulatory network. Besides, subsequent studies to further investigate the *in vivo* synergistic therapeutic mechanisms of the drug through metabolomics and *in vivo* experiments are also needed. By pursuing these research directions, we aimed to expand the scope of the current study, laying a foundation for further research and the clinical application of ZSQS in the treatment of skeletal muscle injury.

4 Conclusion

In this study, a comprehensive methodological framework was employed to identify the therapeutic targets and mechanisms through which ZSQS acts against skeletal muscle injury. Among the bioactive components of ZSQS, quercetin, luteolin, kaempferol, and β-sitosterol have emerged as key functional compounds, with AKT1 identified as a potential core target. These findings emphasize that the therapeutic effectiveness of ZSQS in treating skeletal muscle injury is mainly mediated by enhancing antioxidative and anti-inflammatory responses, processes regulated *via* the AKT/Nrf2 signaling pathway. Additionally, the MAPK and NF-κB signaling pathways are also hypothesized to be closely involved in how ZSQS exerts its protective effects against skeletal muscle injury. Overall, this research highlights the promising potential of ZSQS as a therapeutic agent for skeletal muscle injury, offering valuable insights to researchers and clinicians engaged in developing effective targeted therapies for this condition.

Supplementary Available online (http://www.pibb.ac.cn, http://www.cnki.net):
PIBB_20250421_Table S1.pdf
PIBB_20250421_Table S2.pdf
PIBB_20250421_Table S3.pdf
PIBB_20250421_Table S4.xlsx
PIBB_20250421_Table S5.xlsx
PIBB_20250421_Table S6.xlsx
PIBB_20250421_Table S7.pdf
PIBB_20250421_Table S8.pdf
PIBB_20250421_Table S9.pdf
PIBB_20250421_Figure S1.pdf
PIBB_20250421_Figure S2.pdf
PIBB_20250421_Figure S3.pdf
PIBB_20250421_Figure S4.pdf
PIBB_20250421_Figure S5.pdf
PIBB_20250421_Figure S6.pdf
PIBB_20250421_Figure S7.pdf
PIBB_20250421_Figure S8.pdf

References

[1] Sweeney H L, Hammers D W. Muscle contraction. Cold Spring Harb Perspect Biol, 2018, **10**(2): a023200
[2] Warren G L, Ingalls C P, Lowe D A, *et al*. Excitation-contraction uncoupling: major role in contraction-induced muscle injury. Exerc Sport Sci Rev, 2001, **29**(2): 82-87
[3] Tu H, Li Y L. Inflammation balance in skeletal muscle damage and repair. Front Immunol, 2023, **14**: 1133355
[4] Brieger K, Schiavone S, Miller F J, *et al*. Reactive oxygen species: from health to disease. Swiss Med Wkly, 2012, **142**: w13659
[5] Ji L L. Antioxidant signaling in skeletal muscle: a brief review. Exp Gerontol, 2007, **42**(7): 582-593
[6] Mittal M, Siddiqui M R, Tran K, *et al*. Reactive oxygen species in inflammation and tissue injury. Antioxid Redox Signal, 2014, **20**(7): 1126-1167
[7] Dueweke J J, Awan T M, Mendias C L. Regeneration of skeletal muscle after eccentric injury. J Sport Rehabil, 2017, **26**(2): 171-179
[8] Harirforoosh S, Asghar W, Jamali F. Adverse effects of nonsteroidal antiinflammatory drugs: an update of gastrointestinal, cardiovascular and renal complications. J Pharm Pharm Sci, 2013, **16**(5): 821-847
[9] Turnagöl H H, Koşar Ş N, Güzel Y, *et al*. Nutritional considerations for injury prevention and recovery in combat sports. Nutrients, 2021, **14**(1): 53
[10] Siu W S, Ma H, Cheng W, *et al*. Traditional Chinese medicine for topical treatment of skeletal muscle injury. Pharmaceuticals, 2023, **16**(8): 1144
[11] Cao X. Toxicological experiment research of the effect of different doses of Zheng's sanqisan notogin-seng powder on animal's renal cell. J Chengdu Sport Univ, 2015, **41**(4): 118-121
[12] Ran D Z, Lan Z X, Li K, *et al*. Selected Medical Writings of Zheng Huaixian. Chengdu: Sichuan University Press, 1998: 107-108
[13] Peerzada A M, Ali H H, Naeem M, *et al*. *Cyperus rotundus* L.: traditional uses, phytochemistry, and pharmacological activities. J Ethnopharmacol, 2015, **174**: 540-560
[14] Kilani-Jaziri S, Neffati A, Limem I, *et al*. Relationship correlation of antioxidant and antiproliferative capacity of *Cyperus rotundus* products towards K562 erythroleukemia cells. Chem Biol Interact, 2009, **181**(1): 85-94
[15] Wang T, Guo R, Zhou G, *et al*. Traditional uses, botany, phytochemistry, pharmacology and toxicology of *Panax notoginseng* (Burk.) F.H. Chen: a review. J Ethnopharmacol, 2016, **188**: 234-258
[16] Choi R C, Jiang Z, Xie H Q, *et al*. Anti-oxidative effects of the biennial flower of *Panax notoginseng* against H_2O_2-induced cytotoxicity in cultured PC12 cells. Chin Med, 2010, **5**: 38
[17] Wahab S, Annadurai S, Abullais S S, *et al*. *Glycyrrhiza glabra* (licorice): a comprehensive review on its phytochemistry, biological activities, clinical evidence and toxicology. Plants, 2021, **10**(12): 2751
[18] Jiang J, Zhang X, True A D, *et al*. Inhibition of lipid oxidation and rancidity in precooked pork patties by radical-scavenging licorice (*Glycyrrhiza glabra*) extract. J Food Sci, 2013, **78**(11): C1686-C1694
[19] Brooks S V. Current topics for teaching skeletal muscle physiology. Adv Physiol Educ, 2003, **27**(1/2/3/4): 171-182
[20] Zhang Y, Fu K, Wang C, *et al*. Protective effects of dietary quercetin on cerebral ischemic injury: pharmacology, pharmacokinetics and bioavailability-enhancing nanoformulations. Food Funct, 2023, **14**(10): 4470-4489
[21] Xu X R, Yu H T, Yang Y, *et al*. Quercetin phospholipid complex significantly protects against oxidative injury in ARPE-19 cells

associated with activation of Nrf2 pathway. Eur J Pharmacol, 2016, **770**: 1-8

[22] Dong F, Wang S, Wang Y, *et al*. Quercetin ameliorates learning and memory *via* the Nrf2-ARE signaling pathway in d-galactose-induced neurotoxicity in mice. Biochem Biophys Res Commun, 2017, **491**(3): 636-641

[23] Li L, Jiang W, Yu B, *et al*. Quercetin improves cerebral ischemia/reperfusion injury by promoting microglia/macrophages M2 polarization *via* regulating PI3K/Akt/NF-κB signaling pathway. Biomed Pharmacother, 2023, **168**: 115653

[24] Zaplatic E, Bule M, Ali Shah S Z, *et al*. Molecular mechanisms underlying protective role of quercetin in attenuating Alzheimer's disease. Life Sci, 2019, **224**: 109-119

[25] Cheung S, Zhong Y, Wu L, *et al*. Mechanism interpretation of Guhan Yangshengjing for protection against Alzheimer's disease by network pharmacology and molecular docking. J Ethnopharmacol, 2024, **328**: 117976

[26] Chen J, Ye W. Molecular mechanisms underlying Tao-Hong-Si-Wu decoction treating hyperpigmentation based on network pharmacology, Mendelian randomization analysis, and experimental verification. Pharm Biol, 2024, **62**(1): 296-313

[27] Ni Q H, Li C H, Yang J J, *et al*. The key components and the mechanism of the synergistic effect of the Ephedra-Gui Zhi pair in the treatment of bronchitis were studied based on network pharmacology. Chin Tradit Pat Med, 2021, **43**(1): 246-254

[28] MENG Y. A transcriptome-based analysis reveals the role of hedgehog signaling in regulating slow muscle autophagy in Chinese perch. Reprod Breed, 2025, **5**(3): 125-134

[29] Gao S J, Li D Y, Liu D Q, *et al*. Dimethyl fumarate attenuates pain behaviors in osteoarthritis rats *via* induction of Nrf2-mediated mitochondrial biogenesis. Mol Pain, 2022, **18**: 17448069221124920

[30] Le A C T, Fiuza-Fernandes J, Silva J M, *et al*. Pretreatment with dimethyl fumarate prevents chronic pain and its comorbidities *via* Nrf2 pathway in a rat model of neuropathic pain. Brain Behav Immun, 2025, **128**: 725-736

[31] Armstrong R B, Ogilvie R W, Schwane J A. Eccentric exercise-induced injury to rat skeletal muscle. J Appl Physiol Respir Environ Exerc Physiol, 1983, **54**(1): 80-93

[32] Kyparos A, Sotiriadou S, Mougios V, *et al*. Effect of 5-day vitamin E supplementation on muscle injury after downhill running in rats. Eur J Appl Physiol, 2011, **111**(10): 2557-2569

[33] Hyldahl R D, Xin L, Hubal M J, *et al*. Activation of nuclear factor-κB following muscle eccentric contractions in humans is localized primarily to skeletal muscle-residing pericytes. FASEB J, 2011, **25**(9): 2956-2966

[34] Pedersen B K, Febbraio M A. Muscle as an endocrine organ: focus on muscle-derived interleukin-6. Physiol Rev, 2008, **88**(4): 1379-1406

[35] Manning B D, Toker A. AKT/PKB signaling: navigating the network. Cell, 2017, **169**(3): 381-405

[36] Ceci R, Maldini M, Olson M E, *et al*. Moringa oleifera leaf extract protects C2C12 myotubes against H_2O_2-induced oxidative stress. Antioxidants, 2022, **11**(8): 1435

[37] Wong S W, Sun S, Cho M, *et al*. H_2O_2 exposure affects myotube stiffness and actin filament polymerization. Ann Biomed Eng, 2015, **43**(5): 1178-1188

[38] Li G, Shang L, Wang X, *et al*. Whey protein mitigates oxidative stress injury and improves protein synthesis in mouse skeletal muscle by regulating the SIRT1/Nrf2/HO-1 axis and AMPK/TSC2/mTOR/4EBP1 pathway. J Food Sci, 2025, **90**(7): e70286

[39] Scannevin R H, Chollate S, Jung M Y, *et al*. Fumarates promote cytoprotection of central nervous system cells against oxidative stress *via* the nuclear factor (erythroid-derived 2)-like 2 pathway. J Pharmacol Exp Ther, 2012, **341**(1): 274-284

[40] da Silva M O L, Figueiredo C M, Neris R L S, *et al*. Chikungunya and mayaro viruses induce chronic skeletal muscle atrophy triggered by pro-inflammatory and oxidative response. Int J Mol Sci, 2024, **25**(16): 8909

[41] Zhang Q, Yao M, Qi J, *et al*. Puerarin inhibited oxidative stress and alleviated cerebral ischemia-reperfusion injury through PI3K/Akt/Nrf2 signaling pathway. Front Pharmacol, 2023, **14**: 1134380

[42] Platonova N, Manzo T, Mirandola L, *et al*. PI3K/AKT signaling inhibits NOTCH1 lysosome-mediated degradation. Genes Chromosomes Cancer, 2015, **54**(8): 516-526

[43] Lin Y, Zhu X, Li Y, *et al*. LY294002 ameliorates psoriatic skin inflammation in mice *via* blocking the Notch1/Hes1-PTEN/AKT/IL-17A feedback loop. Clin Exp Immunol, 2023, **213**(1): 114-124

[44] Bellezza I, Giambanco I, Minelli A, *et al*. Nrf2-Keap1 signaling in oxidative and reductive stress. Biochim Biophys Acta Mol Cell Res, 2018, **1865**(5): 721-733

[45] Pedersen B K, Ostrowski K, Rohde T, *et al*. The cytokine response to strenuous exercise. Can J Physiol Pharmacol, 1998, **76**(5): 505-511

[46] Kevil C G, Pruitt H, Kavanagh T J, *et al*. Regulation of endothelial glutathione by ICAM-1: implications for inflammation. FASEB J, 2004, **18**(11): 1321-1323

[47] Li J, Wang T, Liu P, *et al*. Hesperetin ameliorates hepatic oxidative stress and inflammation *via* the PI3K/AKT-Nrf2-ARE pathway in oleic acid-induced HepG2 cells and a rat model of high-fat diet-induced NAFLD. Food Funct, 2021, **12**(9): 3898-3918

[48] Cai F F, Bian Y Q, Wu R, *et al*. Yinchenhao decoction suppresses rat liver fibrosis involved in an apoptosis regulation mechanism based on network pharmacology and transcriptomic analysis. Biomed Pharmacother, 2019, **114**: 108863

[49] Weng C J, Chen M J, Yeh C T, *et al*. Hepatoprotection of quercetin against oxidative stress by induction of metallothionein expression through activating MAPK and PI3K pathways and enhancing Nrf2 DNA-binding activity. N Biotechnol, 2011, **28**(6): 767-777

[50] Jo H, Mondal S, Tan D, *et al*. Small molecule-induced cytosolic activation of protein kinase Akt rescues ischemia-elicited neuronal death. Proc Natl Acad Sci USA, 2012, **109**(26): 10581-10586

基于生物信息学预测、化学分析及实验验证探究郑氏三七散治疗骨骼肌损伤的作用机制*

王鼎锐[1)]　刘芸欣[1)]　徐俊杰[2)]　杨　柳[1)]　吕家豪[1)]　邢程远[1)]　闫　磊[1)**]　郗蓓蓓[1)**]

（[1)] 成都体育学院，运动医学四川省重点实验室，运动医学与健康研究所，运动医学与健康学院，成都 641418；
[2)] 成都医学院临床医学院，成都 610500）

摘要　目的　郑氏三七散（Zheng’s San Qi San，ZSQS）是用于治疗肌肉、肌腱、韧带等软组织损伤的经典中医药方剂，但其治疗机制尚未明确。本研究旨在筛选并鉴定ZSQS中的药效活性成分及其候选生物分子靶点，进一步阐明该方剂治疗骨骼肌损伤的分子机制。**方法**　采用网络药理学方法构建“ZSQS-成分-靶点”、“蛋白质相互作用（PPI）”以及“活性成分-核心靶点-通路”网络，预测ZSQS治疗骨骼肌损伤的关键成分和潜在核心靶点，并通过GEO数据库的基因芯片分析数据验证这些预测结果。随后，通过分子对接技术评估筛选出的活性成分与候选核心靶点的结合能力，并利用液相色谱-质谱联用技术（LC-MS）对ZSQS及含药血清活性成分进行定性和定量分析验证。最后，借助离心运动骨骼肌损伤动物模型和氧化应激肌管细胞损伤模型，验证ZSQS的临床疗效及其对关键靶点生物学功能的调控干预效果，进而明确其潜在治疗机制。**结果**　在ZSQS中鉴定的111种活性成分和其对应的204个骨骼肌损伤修复相关靶点中，筛选出包括AKT1在内的14个核心靶点，以及槲皮素、木樨草素、山柰酚、β谷甾醇4个核心活性成分，在含药血清中也检测到槲皮素、木樨草素、山柰酚3种核心成分的代谢产物。在核心靶点中，*IL-6*、*CASP3*、*HIF1A*、*STAT3*、*JUN*等5个候选基因与基因芯片差异表达筛选结果重合，并且IL-6被证明富集于PI3K/AKT通路。结合AKT1表达水平预测结果推测，AKT1的磷酸化水平在ZSQS的治疗机制中发挥核心作用。分子对接分析进一步提示AKT1的PH结构域与所有4种已通过质谱验证的核心活性成分都具有较高的结合能。最后，动物模型研究显示了ZSQS给药对骨骼肌损伤修复的促进作用及其可能的抗氧化损伤机制，细胞模型研究进一步从机制上证明ZSQS含药血清，核心活性成分联合用药及槲皮素单体可提高AKT磷酸化水平，促进Nrf2核转位，上调下游抗氧化酶（SOD、GPx、GR）的表达，并抑制炎症因子（IL-6、TNF-α）的表达，从而减轻氧化应激与炎症反应。**结论**　ZSQS主要通过激活AKT/Nrf2信号通路，增强细胞抗氧化和抗炎能力，减轻骨骼肌损伤。本研究结果为ZSQS的临床应用及现代化开发提供了科学依据。

关键词　郑氏三七散，骨骼肌损伤，AKT1，Nrf2，抗氧化，抗炎
中图分类号　R285　　**DOI**：10.3724/j.pibb.2025.0421　　**CSTR**：32369.14.pibb.20250421

* 四川省科技教育联合基金（2025NSFSC2102），四川省大学生创新创业项目（S202510653119）和成都体育学院科研卓越计划（2025-A007）资助。
** 通讯联系人。
闫磊　Tel：028-85095776，E-mail：lyulei@cdsu.edu.cn
郗蓓蓓　Tel：028-85593740，E-mail：qiebeibei@cdsu.edu.cn
收稿日期：2025-09-25，接受日期：2026-01-21